Journal of Magnetism and Magnetic Materials 504 (2020) 166653

Contents lists available at ScienceDirect

Journal of Magnetism and Magnetic Materials

journal homepage: www.elsevier.com/locate/jmmm

Research articles

A first-principles study of Mg/Ni induced magnetic properties of $Zn_{0.95-x}Mg_xNi_{0.05}O$

I.P. Duru[a], E. Ozugurlu[b], L. Arda[c,*]

[a] Marmara University, Faculty of Science and Arts, Department of Physics, 35722 Istanbul, Turkey
[b] Istanbul Technical University, Faculty of Science and Letters, Department of Mathematics, 35469 Istanbul, Turkey
[c] Bahcesehir University, Faculty of Engineering and Naturel Sciences, Department of Mechatronic Engineering, 35359 Besiktas, Istanbul, Turkey

ARTICLE INFO

Keywords:
Mg/Ni doped ZnO
First-principles
Nanostructures
Ab-initio calculations
Electronic property
Magnetic property
Density functional theory
Perdew–Burke–Ernzerhof
Generalized gradient approximation

ABSTRACT

Magnetic properties of Mg/Ni doped ZnO were investigated by the first-principles study. The generalized gradient approximation (GGA) in Perdew–Burke–Ernzerhov of the scheme as a form of density functional theory (DFT) utilizing the plane-wave pseudo-potential method was used. Calculations were performed for a constant Ni doping ratio as 5% and different concentrations of Mg varying from 1% to 5%. It was shown that Mg concentrations helped to tune band gap and mediate the ferromagnetic property. 1% Mg-doped structure had a half-metallic ferromagnetic (HMF) state. Meanwhile, metallic behavior (MB) was observed for higher concentrations of Mg (> 1%) impurities. It was revealed that Mg-doped ZnNiO possesses ferromagnetic behavior solely for 1% Mg while other doping ratios were showing distinctive phases including antiferromagnetism (AFM). Besides, there is no evidence of a clear connection between the doping concentration of the Mg and the magnetic phase. Ni distant/near oxygen vacancies (V_o) enhanced the FM state; however, distant vacancies led to HMF state for all Mg concentrations. Zn-d, O-p, and Ni-d (dominates) control the spin-up/down channels by hybridization.

1. Introduction

Due to its interesting electrical, optical, mechanical, and magnetic properties, a big effort has been given to study zinc oxide for the last twenty years. ZnO exhibits a large excitation binding energy, an inherently n-type II-VI semiconductor with a wide band gap, a refractive index, high thermal conductivity and photoconductivity [1–6]. The application fields include optoelectronic devices, solar cells [3], transparent conductor [4], UV-absorbing material in sunscreens [5], the active material in varistors [6], catalysts, chemical sensors, piezoelectric transducers, etc. ZnO can be incorporated into different morphologies including nanoparticles, nanowires, nanorods [1,2]. Moreover, ZnO nanomaterials are favorable candidates for photonics and nanoelectronics.

ZnO materials having a high Curie temperature are potential materials for the diluted magnetic semiconductors (DMS) and DMS doped with varying transition metal (TM) exhibits varying magnetic properties [7–9]. Sato et al. [10] have researched transition metal atoms (Mn, V, Cr, Fe, Co, Ni) doped ZnO materials through first-principle calculations, and they found that the doping system had ferromagnetic (FM) properties. Ueda et al. [11] magnificently prepared 3d transition metal doped ZnO thin film materials. Recent studies showed that in order to improve device technologies such as magnetic memories (MRAM), spin LED, logic devices zinc oxide semiconductors must be doped with different transition metals and elements using magnetic chemical assets at room temperature (RT) [12–14].

Ni-doped ZnO material researches showed that at RT this material had FM property with different preparation techniques such as the sol-gel technique [15], the pulsed laser deposition (PLD) [16]. Cui et al. [17] synthesized Ni- and Co-doped ZnO nanowire arrays with an electrochemical method at 90°C, and they found that magnetic nanowires have anisotropic FM properties. He et al. [18] prepared Ni-doped ZnO nanowire arrays by means of metal vapor vacuum arc (MEVVA) ion source doping technology and pointed out that the electron transport ability increased by 30 times and the absorption peak exhibits red-shift phenomena. Wakano et al. [19] synthesized Ni-doped ZnO thin film materials and found that FM features appeared at 2 K, while PM properties appeared at 300 K. Al-Harbi [20] synthesized a $Zn_{1-x}Ni_xO$ nanorod with excellent UV emissive power by means of a low-temperature hydrothermal method. Cheng et al. [21] prepared a $Zn_{1-x}Ni_xO$ nanorod at RT FM features by means of a low-temperature hydrothermal method. On the contrary, Yin et al. [22] reported that no FM feature was observed in $Zn_{1-x}Ni_xO$ nanomaterials.

Arda et al. [23] showed that the existence of ferromagnetism in

* Corresponding author.
E-mail address: lutfi.arda@bau.edu.tr (L. Arda).

https://doi.org/10.1016/j.jmmm.2020.166653
Received 8 April 2019; Received in revised form 13 February 2020; Accepted 21 February 2020
Available online 22 February 2020

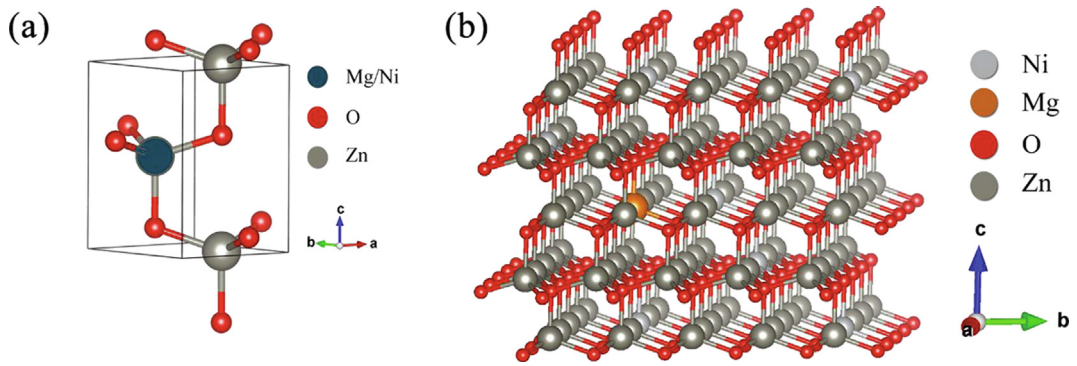

Fig. 1. A sample cell to illustrate atomic locations (Mg, Ni, O, and Zn) (a) unit cell (b) 5 × 5 × 2 supercell: Mg(1%)/Ni(5%) ions were replaced to host Zn.

Ni^{2+} doped ZnO does not only depend on lattice defects but also on growth techniques. Dogan et al. [24] pointed out that the grain sizes of the ZnNiO nanoparticles were measured to be approximately 90 nm by means of a Scanning Electron Microscope (SEM). The XRD and SEM measurements showed that Ni-doped ZnO had wurtzite structures with NiO secondary phases. RT ferromagnetism was observed for highly Ni-doped ZnO nanoparticles. Heiba et al. [25] founded that $NiFe_{2-x}Gd_xO_4$ ($0.0 \leq x \leq 0.4$) nanoferrites exhibited superparamagnetic behavior at RT while pure nickel ferrite exhibited ferromagnetic (FiM) behavior. The saturation of magnetization (Ms) at 10 K first decreased due to the presence of Gd ions in A site, after that it increased as the amount of Gd substitution increased due to substitution of Fe^{3+} ions by Gd^{3+} ions which had a larger magnetic moment. The coercive field increased with the Gd content due to the decrease in crystallite size.

Viswanatha et al. [26] produced Mg-doped ZnO nanoparticles in the range of 60–90 nm and they found that the morphology structure changed when the concentration of dopant was increased. In our previous work, it was pointed out that as Mg concentration value increased, the magnetization decreased considerably and the loop M − H curve at 300 K exhibited the strong ferromagnetism in $Zn_{0.94}Mg_{0.01}Ni_{0.05}O$ nanoparticles in the range of 24–27 nm within 0.01% and 0.05% of Mg [7]. It was concluded that the size and shape of the nanoparticles depended on the preparation materials and methods [27]. El Foulani et al. [28] produced $Co_{0.5}Zn_{0.5}Fe_2O_4$ spinel ferrite nanoparticles by a novel synthetic technique and showed that the saturation magnetization and remanent magnetization increased gradually as the crystallite size decreased, although all samples were well above the reported critical grain sizes of ~ 20–25 nm for CFO by Rajendran et al. [29]. They also contributed a useful theoretical basis for the application of ZnO DMSs. Vachani et al. [30] deduced that the concentration of oxygen vacancies is not the only important parameter for the occurrence of ferromagnetism in Cu:ZnO but that the position of oxygen vacancies also plays an important role. Single-crystalline ZnNiO nanoparticles were produced to investigate room temperature FM originating from oxygen vacancies and magnetic polaron formation [31].

The structural, electronic and magnetic properties of Mg/Ni doped ZnO for various concentrations by DFT calculations based on generalized gradient approximation (GGA) with PBE scheme were investigated. Mg was doped to the system instead of Zn atoms up to 5% and Ni concentration was chosen as 5%. Origins of magnetism and electronic behavior that were mediated by intrinsic effects such as structural formation (variation of bond lengths, bond angles and dihedral angles) and orbital hybridizations were revealed including Ni distant/near oxygen vacancies in which spin density intrinsically changed causing orbital hybridizations and unpaired electrons.

2. Model and method

CASTEP [32] was used to perform DFT calculations with a generalized gradient approximation (GGA) in the Perdew-Burke-Ernzerhof (PBE) scheme to investigate electronic and magnetic properties of Mg/Ni doped ZnO for different doping concentrations of Mg. The functional from the Generalized Gradient Approximation (GGA) of PBE [33] was chosen due to its good description of chemical bond energies. Ni doping ratio was fixed at 5%. Electron-ion interactions were represented by an ultra-soft pseudopotential with Koelling-Harmon relativistic treatment and energy cut-off was set to 380 eV. Electronic configurations of corresponding atoms Zn, Mg, Ni, and O, in short, valance configurations were treated as 3 *s*2, 3*d*10 4 *s*2, 3*d*8 4 *s*2 and 2 *s*2 2*p*4, respectively. 5 × 5 × 2 packed $Zn_{0.95-x}Mg_xNi_{0.05}O$ supercell was constructed via implementing the lattice parameters, a(Å) and c (Å) of experimental results which were reported by our previous work [7]. Ni/Mg ions were interchanged with host Zn sites to achieve the desired doping concentration of Mg/Zn, at the same time, corresponding a(Å) c(Å) values were updated with following experimental values; bond lengths, bond angles and dihedral angles which were calculated for certain (Ni: 5%, Mg: 1–5%) doping concentrations since they crucially affected the type of exchange interactions, for instance, indirect exchange such as super-exchange integral due to the overlapped orbitals of atoms. SCF and band energy tolerance were set to 1e − 4 eV/cell and 1e − 5 eV, respectively. A 200 atoms (100 Zn and 100 O) wurtzite hexagonal supercell was adopted to deal with very low concentrations of dopants, especially 1% of Mg as shown in Fig. 1.

3. Results and discussion

Magnetic characterization of ZnMgNiO nanoparticles has been previously carried out by our earlier work [7] experimentally and a theoretical investigation on the size-dependent magnetic behavior of these particles was evaluated by our previous work [34] resulting in a critical range of size that FM strongly existed. The authors focused on another inclusive explanation of the origin of FM attitude that largely supports the previous explanations via first-principles calculations. There are remarkable interpretations such as super-exchange (SE), double-exchange (DE) and orbital hybridizations to explain how DMS materials show magnetic behavior, especially FM or FiM, through an ultra-low doping ratio. Mg and Ni ions were replaced with a quite distance Zn both randomly since it was aimed to avoid the explicit contribution of Mg and/or Ni clusters. Experimental lattice parameters allowed us to build ZnMgNiO supercell and to calculate bond angles and lengths corresponding to certain Mg concentrations of 1–5% with fixed Ni concentration (5%) during the calculations. Total energy, Fermi energy, Metallic Behavior (MB) and integrated spin density including experimental lattice parameters were given in Table 1. As seen in Table 1, the total energies increased as Mg concentration increased. The Fermi energy appeared only at 1% Mg concentration which had the lowest total energy and a Half-Metallic (HM) behavior.

However, structural properties, such as bond angles and lengths, were exhibited in Table 2. In this context, they likely to control electrical activities that restrain/guide charge transport, and on the other

Table 1
Experimental lattice parameters and calculated energies and metallic behavior (Met. B) corresponding to Mg concentrations of 1–5%.

Mg (%)	1	2	3	4	5
a(Å)	3.23	3.24	3.255	3.244	3.253
c(Å)	5.206	5.204	5.201	5.200	5.195
Total Energy (eV)	−212200.248	−211466.838	−210733.651	−209998.500	−209266.426
Energy/p.a. (eV)	−1061.001	−1057.334	−1053.668	−1049.993	−1046.332
Fermi Energy (eV)	4.672	–	–	–	–
MB	HM	M	M	M	M

Table 2
Bond lengths of Ni-Ni, Ni-O, Mg-O, Ni-Zn, Mg-Zn and Mg-Ni; bond angles of Zn-Zn, Ni-Zn and Mg-Zn through oxygen.

Contact/Connection	Bond lengths (Å)
Ni-Ni	3.208
Ni/Mg-O	1.972
Ni/Mg-Zn	3.207
Mg-Ni	4.567
	Bond angles (°)
Zn-O-Zn	110.860
Ni-O-Zn	110.860
Mg-O-Zn	108.044

hand, essentially localized electrons depend on the atomic distances indicating indirect exchange mechanisms that possess intriguing rationality in explanation of FM. Direct exchange interactions between Ni ions take place at a distance that is longer than nearest Ni-O, Zn-O and Mg-O couples. Whether strength and the sign of the exchange energy J is a major fact on the determination of mean magnetic behavior and can be properly calculated via those direct interactions, indirect mechanisms play a crucial role to bring out the hybridizations p-d, s-p and etc. generally mediated by oxygen in oxides. It can be inferred that they may not specifically contribute to FM even determining the magnetic state.

Spin-polarized total DOS (TDOS) and partial DOS (PDOS) of the system were figured out to discover the electronic and magnetic properties according to the doping ratio. We briefly glanced at 5% Ni-doped ZnO. O(*2p*)-Ni(*3d*) hybridization and a variation in up/down electrons were found to be the major reasons for spontaneous magnetization inducing an FM behavior. Note that these results agree with previous studies [35,36]. However, it can be clearly seen that Ni-*3d* and O-*2p* contributed to the states in a wide energy range between −7.2 eV and −0.47 eV as shown in Fig. 2. Ni-*3d* is the dominant state in the energies from −2 eV up to the 0.56 eV close to Conduction Band Minima (CBM). In the down spin case, Ni-*3d* and weak O-*2p* contributed between −0.32 eV and 0.56 eV occupying the Fermi level.

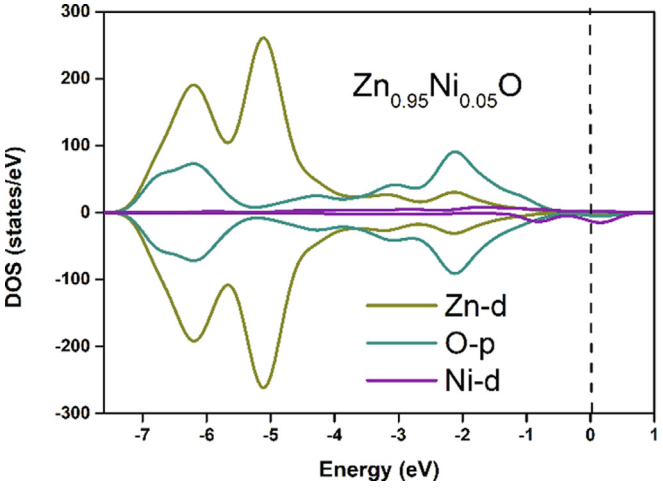

Fig. 2b. PDOS of 5% Ni doped ZnO ($Zn_{0.95}Ni_{0.0}O$):Zn(3*d*), O(*2p*) and Ni(*3d*).

Doping Mg conduced to a reasonable number of states occurred for all concentrations in Conduction Band (CB) energies especially bigger than 1 eV and did not differ practically from one another. TDOS of 1–5% Mg-doped ZnNiO were shown in Fig. 3 except for 2% Mg (see it in supplementary data). In Fig. 2a, a wide band gap of ~2 eV between Valance Band (VB) and CB depicted a semiconducting state for a spin-up channel; simultaneously, an oval-shaped line appeared surrounding the center of the Fermi level fora spin-down channel which pointed out a metallic state. In other words, 1% Mg doping caused a metallic attitude to the material even though it was metal for higher concentrations. Fig. 3(b), (c), and (d) explicitly confirmed the latter one. Besides, a perfectly symmetrical appearance in TDOS energies existed during the

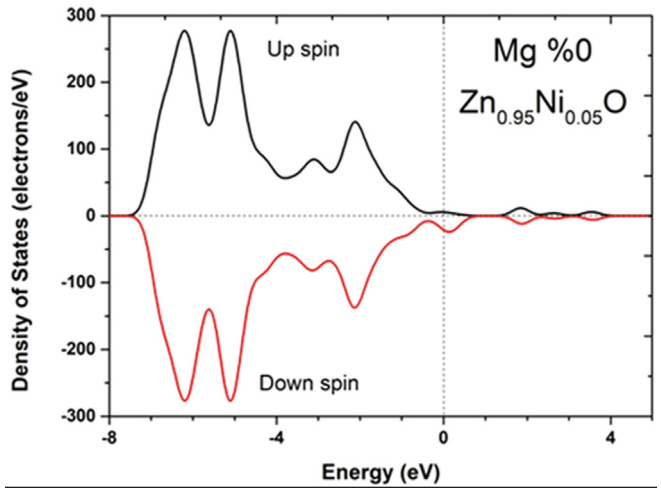

Fig. 2a. TDOS of 5% Ni doped ZnO ($Zn_{0.95}Ni_{0.0}O$).

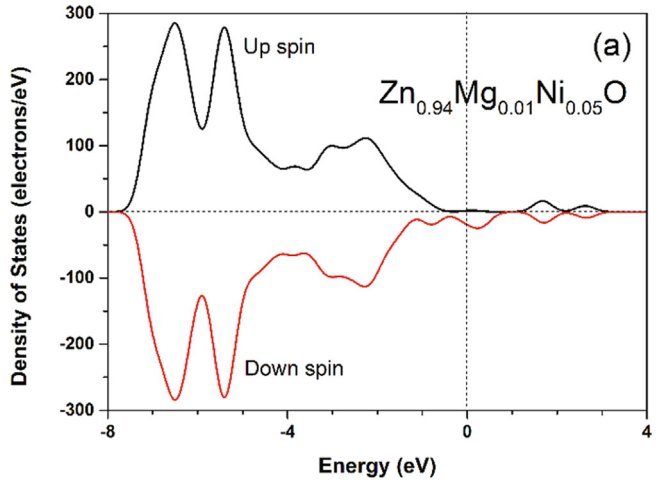

Fig. 3. TDOS of$Zn_{0.95-x}Mg_xNi_{0.05}O$ for × values as (a) 0.01, (b) 0.02, (c) 0.03, (d) 0.04, and (e) 0.05.

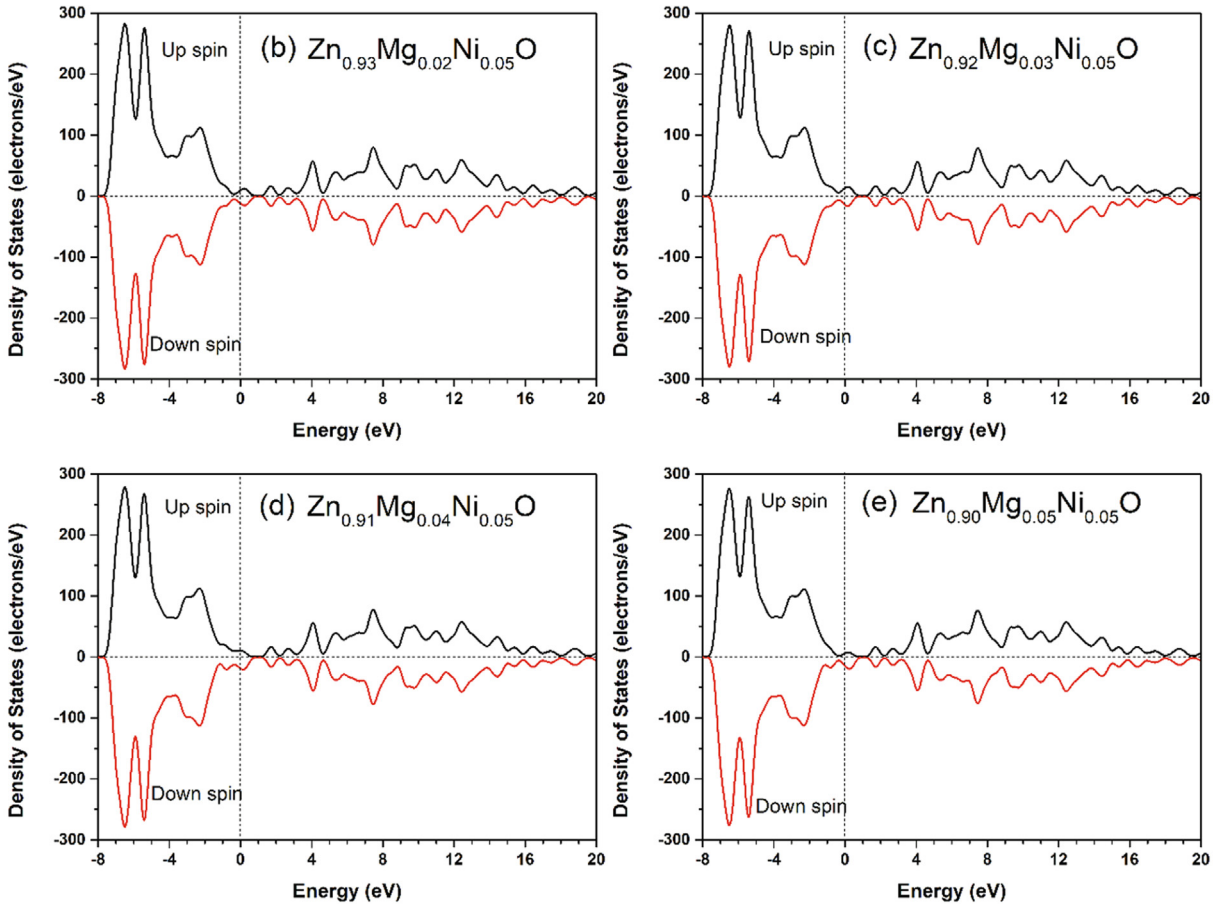

Fig. 3. (*continued*)

overlapping bands (CB and VB) introducing a zero Fermi energy for x > 1 while GGA calculations of 1% Mg-doped structure leads the system having 4.672 eV Fermi energy.

Table 3 shows integrated spin densities and determined magnetic states of the material for corresponding Mg concentrations. It could be deduced that 1% Mg-doped ZnNiO was FM and the others showed very weak FiM behavior except for 3% doped Antiferromagnetic (AFM) one according to its low integrated spin density which was so close to zero. In addition, it showed a reversed-bell behavior as shown in Fig. 4. For 3% Mg concentration, majority and minority spin channels had a similar number of electrons around the Fermi level that indicated an AFM phase in contrast to FiM 2% Mg-doped ZnNiO.

As a further interest, we also investigated the individual contribution of atomic orbitals, including hybridizations, and overall magnetic properties of the $Zn_{0.95-x}Mg_xNi_{0.05}O$ with the above-mentioned concentrations of Mg (Fig. 5). Mg-2 *s*, Zn-4 *s*, 4*p* and Ni-4 *s*, 4*p* states jointly contributed to the bottom of VB between energies −19 eV and −18 eV. All states except Zn-3*d* and Ni-3*d* contributed to DOS at 1–3 eV energies in CB. However, the Fermi level was dominated by Ni-3*d* and O-2*p* despite the weak existence of the rest part. Fig. 5 showed that minority spin states of Ni-3*d* and O-2*p* hybridized at the Fermi level. Note that

Table 3
Spin density and magnetic behavior (MB) corresponding to Mg concentrations (1–5%).

Mg (%)	1	2	3	4	5
MB	FM	FiM	AFM	FiM	FiM
Integrated Spin Density (ħ/2)	11.358	2.067	0.061	4.722	6.126
Integrated |Spin Density| (ħ/2)	11.323	11.104	10.347	8.739	11.263

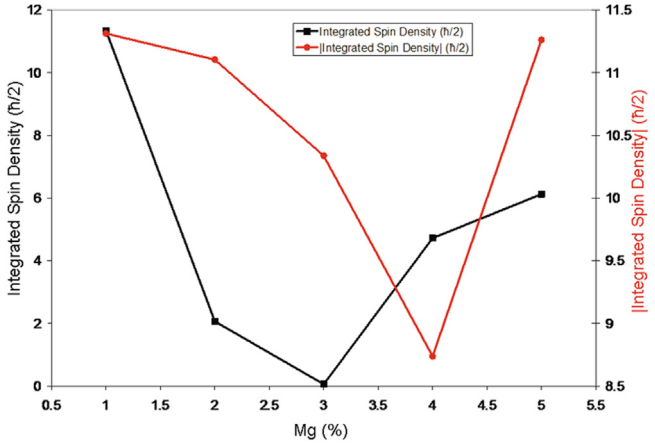

Fig. 4. The integrated spin density of the simulated supercell of 1–5% Mg-doped ZnNiO.

Mg-*s*, Zn-*s*,*p*, and Ni-s, p influenced the density of states at/around Fermi level.

For 1% Mg-doped ZnNiO, the contribution to the density of states was originated from the atomic orbitals of Ni(*s*, *p*), Mg(*s*), and mostly Zn(*s*, *p*) in the energy range −19 eV to −18 eV as illustrated in Fig. 5. Besides, all the atomic orbitals provided a similar contribution between −8 eV and −1 eV except for Ni-*d*. Spin down states of Ni-3*d*, 4*p*, and O-2*p* gave arise to minority spin channels around the Fermi level; in addition, the existence of Ni 4 *s*, 4*p* and Mg 2 *s* was very lower in contrast to others. The dominant contribution in minority spin channels was caused by Ni and O which were definitely hybridized. In the case of 2%

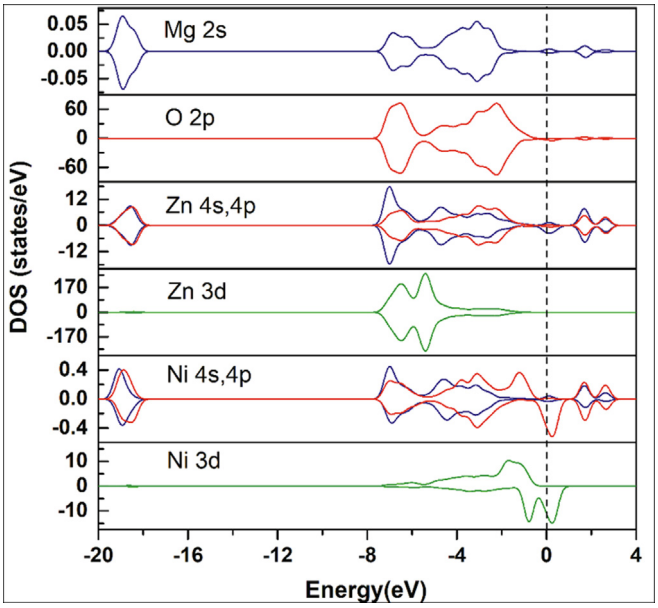

Fig. 5. PDOS of 1% Mg-doped ZnNiO. *s*, *p* and d states were denoted by the navy, red and olive-colored lines, respectively. The dashed line was used to show the Fermi level. The positive value of PDOSs represented up-spin states and negative ones belong to down-spin states. (For interpretation of the references to colour in this figure legend, the reader is referred to the web version of this article.)

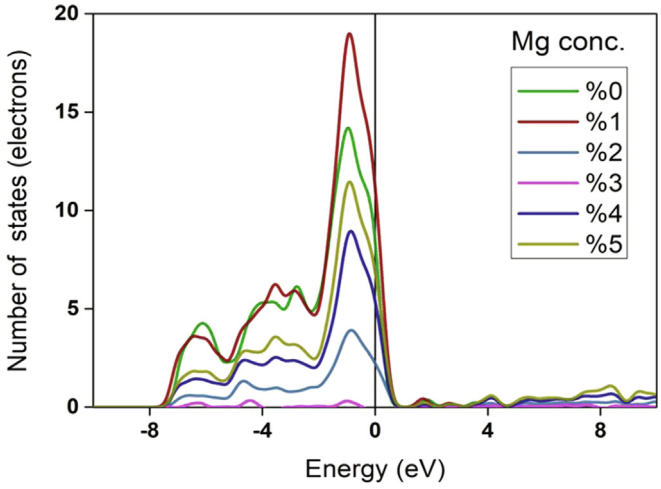

Fig. 6. Number of states (electrons) versus conduction band energy (eV) for all Mg concentrations.

Mg doping, O-*p* and Zn, Mg and a few of Ni(*s*, *p*) contributions were observed and the effect of *d* orbitals disappeared at the Fermi level. Moreover, Zn-*d* and O-*p* enhanced the electronic structure between −19 eV and −7 eV. When 3% Mg is doped to ZnNiO, O-2*p* and Zn-3*d* yielded a similar dominant contribution in the same region; meanwhile, it practically vanished at the depth of VB. Mg, Zn (*s*, *p*), Ni (*s*, *p*), and especially Zn (*s*, *p*) contributed to the sates above the Fermi level, and there was almost no contribution from all the *d* orbitals. Similar results were obtained for 4% and 5% Mg doping ratios as seen in Figs. 8-9. For 3% Mg doping, up and down spin states of all the atomic orbitals showed a *mirror* symmetry which was a typical indication of AFM behavior. The density of states of the down spins was higher than up spins for all the Mg doping ratios except for 3% Mg. Corresponding DOS figures of 2, 3, 4 and 5% Mg-doped ZnNiO were shown in supplementary material labeled as Fig. S1–S4, respective to the increasing doping ratio.

From Fig. 6, the obtained results showed that 1% of Mg-doped ZnNiO had the most number of states (electrons) at the Fermi level showing an FM behavior. On the other hand, the least number of states (electrons) was observed for 3% Mg doping around the Fermi level showing an AFM behavior, but for the other doping ratios (2, 4, and 5%) the number of states changed randomly and showed an FiM behavior. Therefore, the magnetic behavior of the system possessed various phases such as AFM, FM, and FiM.

3.1. Distant/near oxygen vacancies

Vacancies can be expected as defects generated during various experimental processes, they definitely influence the magnetic behavior of the system; in some cases, this introduces a suitable state for the constitution of unpaired electrons which lead FM. In other words, they contribute to a magnetic state of the whole material as an intrinsic impurity. In the case of oxygen vacancies, Weng Zhen-Zhen et al. [37] reported that these defects not only strengthened magnetic coupling between TM ions when vacancy-TM ion distance decreased but also can be responsible for FM behavior in the lack of any other impurity atom/dopant [37–40]. In other words, V_o literally changes the band structure, acting on VBM and CBM values close to the Fermi level, and thus contribute to FM [41,42]. Moreover, oxygen vacancies (V_o) confine electrons, whose orbital wave function overlaps with TM metal d shells, introducing magnetic polarons as well [40]. Therefore, oxygen vacancies distant (V_o^d)/near(V_o^n) to Ni were generated to elaborate the vacancy distance/existence and dependency on the doping concentration of Mg in Mg/Ni co-doped ZnO. Firstly, the location of V_o^d was set to block a probable interaction within the Ni ions, then V_o^n was tuned to be close to Ni provoking Zn (3d) electrons and Zn(*3d*)-O(*2p*) hybridizations [38,39]. In order to elucidate the existence of vacancies to magnetic behavior, DOSs were calculated as detailed in the Method section. 5% Ni-doped ZnO without Mg impurities was introduced to avoid the effect of Mg ion, and TDOS (Zn-(*3d*), O(*2p*) and Ni (3d)), PDOS were given in Fig. 7.

Distant defect configuration (straight line) possesses semi-metallic behavior since majority spins state vanished at a wide range of energies including Fermi level while down spin state occupies at Fermi level. For near defects (short dash) a noticeable variation between channels at E_f introduces an FM like behavior which is observed in a distant defect. However, it is clear that distant defect does not dramatically affect the system even contribution to electronic states at CB region above 2 eV were realized, especially electronic states lying around Fermi level when compared with a non-defected structure in the absence of Mg ion. There is a pretty obvious presence of Ni (*3d*) and O (*2p*) states around Fermi level which also shoulders the responsibility of FM behavior together via orbital hybridization (Fig. 8a) which can be used as a valid explanation for near vacancy case too (Fig. 8b). Despite any immediate contribution of Zn around Fermi level, Zn contributed to the lower eV states at the VB region with O (*2p*) states.

We could not observe such effectiveness of Zn (*3d*) around the Fermi level that can lead us to hold responsible FM in origins so far but Ni (*3d*) – O (*2p*) gave a remarkable contribution in all cases. Nevertheless, quite little electronic effectiveness around the Fermi level of Zn ions may cause a drastic contribution since the number of Zn is outnumber. For a further investigation, we carried out the joint distinct effect of oxygen vacancies and Mg impurities doped to ZnNiO together either distant or near the defect. One can notice that a pretty similar contribution to the density of states had been made during CB and VB regions except around the Fermi level. 1% Mg-doped ZnNiO showed half-metallic behavior for corresponding vacancies.

Despite the favorable configurations that do not linearly relate to Mg concentration, it is clearly definite that total energy decreased regarding the increasing Mg concentration for both distant and near oxygen vacancies. Whole distant oxygen vacancies consistently lead the system to possess an HMF behavior, divergent states occurred in the

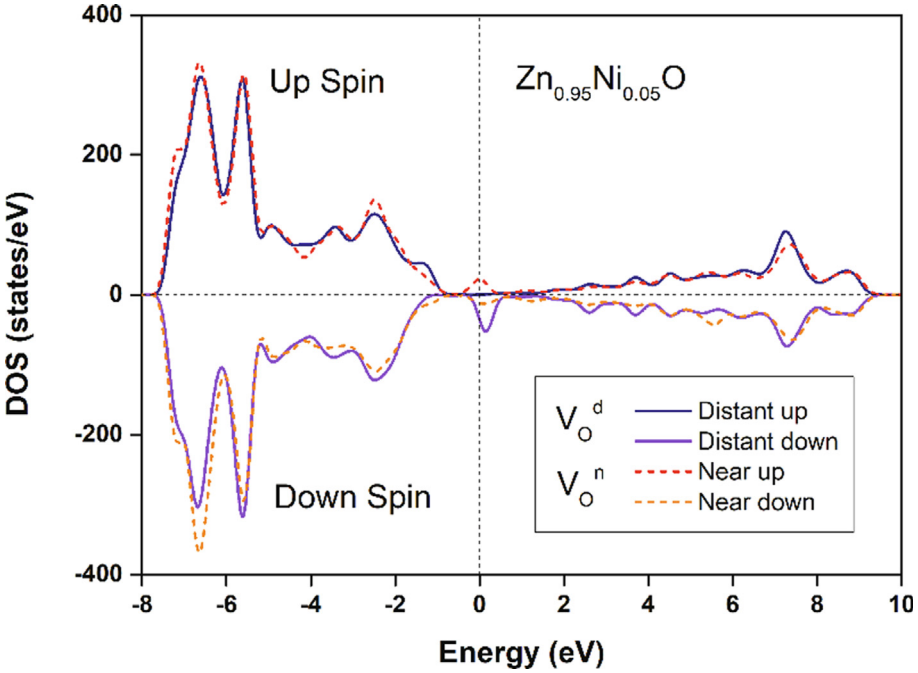

Fig. 7. TDOS of 5% Ni-doped ZnO ($Zn_{0.95}Ni_{0.05}O$): Straight and short dash lines indicate distant (V_o^d) and near (V_o^n) oxygen vacancies, respectively.

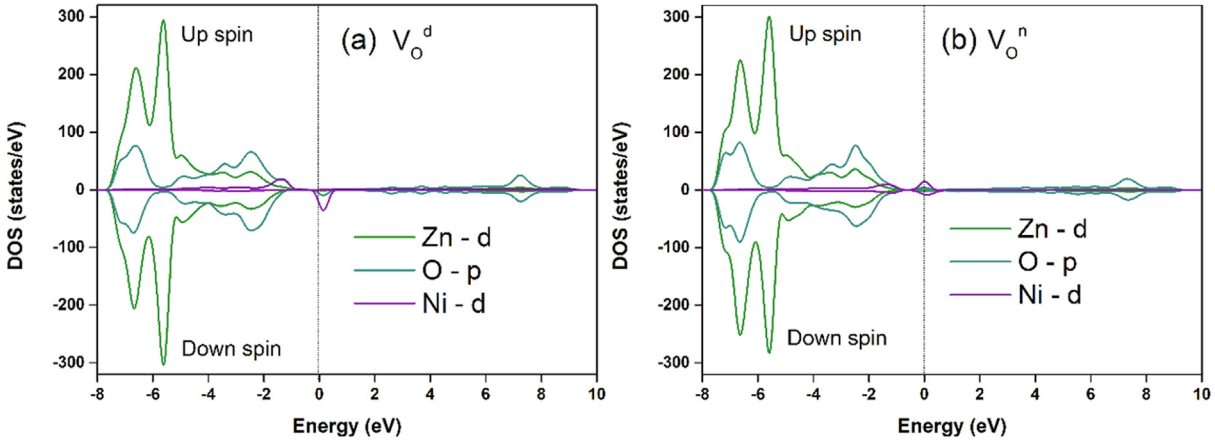

Fig. 8. PDOS of 5% Ni-doped ZnO ($Zn_{0.95}Ni_{0.0}O$):Zn(3d), O(2p) and Ni(3d) in case of (a) distant oxygen vacancy (b) near oxygen vacancy.

presence of near oxygen vacancies. Detailed information about the energies and MB was given in Table 4.

PDOS of 1% Mg-doped ZnNiO was given in Fig. 10 to analyze the atomic and orbital contributions individually. A slight contribution to the Fermi level was made by Zn-*3d* orbital confirming [38–41] according to the PDOS of distant/near of $Zn_{0.95-x}Mg_xNi_{0.05}O$. That is to say, though Ni-*3d* dominates around Fermi level, Zn-*s,p,d*, Ni-*p,d* and O-*p* are both energetic at/around Fermi level in defining the magnetic state. Moreover, Zn-d and O-p donated to lower VB energy herewith Ni-d showed any responsibility for CB and, distant/near vacancies were not different in this manner except possessing separate values on the edge of VB. Distant vacancies introduced minority spin channels while up spins dominated the minority channels in the presence of near vacancies which mostly decided on the magnetic state of the system for 3 and 5% Mg (Fig. S9). However, this led the system to possess an HMF state. Apart from others, 2% Mg near vacancy is actually SC while distant vacancy introduced HMF state. One can deduce that vacancies may control the density of spin channels at/around Fermi level. Corresponding DOS figures of 2, 3, 4 and 5% Mg-doped ZnNiO were shown in supplementary material labeled as Fig. S5–S7, respective to the increasing doping ratio as shown in Table 5.

The positive value of PDOSs represented up-spin states and negative ones belong to down-spin states. Integrated spin densities elaborate on the magnetic state of the system as well. In case of distant vacancies, they are also FM state for all Mg dopants where near vacancies caused to FiM. AFM state disappeared when a few vacancies were added to the structure.

Integrated spin densities give rough information about the magnetic state of the system overall, which means a detailed search is still needed for a deep scan through orbital exploration over spin channels. Table 4 helped us to label the magnetic behavior of the system with a low cost, specifying the FiM states, therefore it can be depicted that distant oxygen vacancies, briefly defects, caused FM states while near defects led the system to gain FiM property for all Mg concentrations. In addition, vacancies tuned the magnetic state especially forming FM and FiM states, since they handled the spin density with neighboring electrons as a remarkable fact.

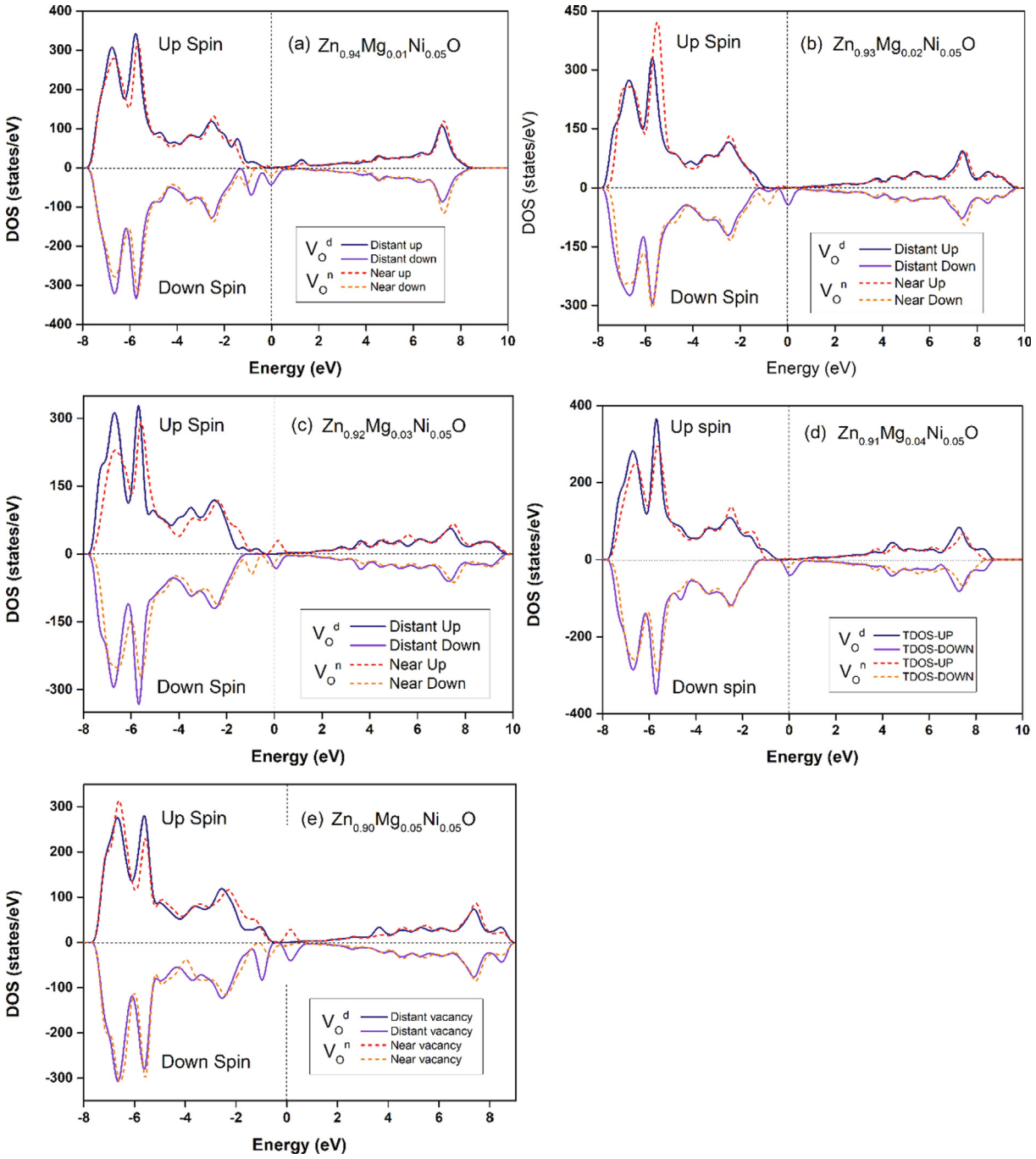

Fig. 9. TDOS of $Zn_{0.95-x}Mg_xNi_{0.05}O$ with distant/near for × values as (a) 0.01, (b) 0.02, (c) 0.03, (d) 0.04, and (e) 0.05. Straight and short dash lines indicate distant (V_o^d) and near (V_o^n) oxygen vacancies, respectively.

Table 4
Calculated energies per atom (TE) and metallic behavior (MB) corresponding to Mg concentrations of 1–5% and distance of oxygen vacancies.

	Mg (%)					
		1	2	3	4	5
TE (eV)	Distant vacancy	−901.846	−904.607	−907.639	−909.489	−912.710
	Near Vacancy	−901.768	−904.668	−907.052	−910.612	−913.340
MB	Distant vacancy	HM	HM	HM	HM	HM
	Near Vacancy	HM	SC	M	HM	M

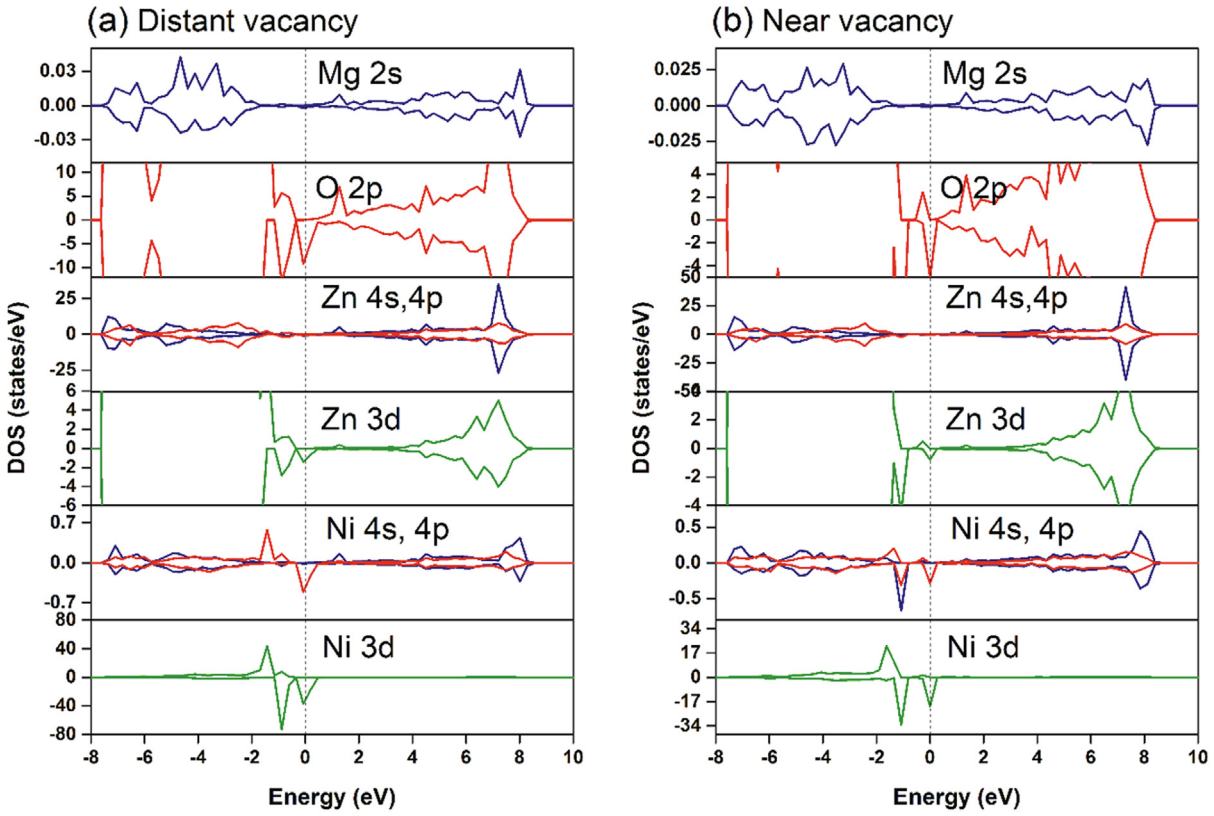

Fig. 10. PDOS of 1% Mg-doped ZnNiO (a) distant vacancy (b) near vacancy *s*, *p* and d states were denoted by the navy, red and olive-colored lines, respectively. The dashed line was used to show the Fermi level.

Table 5
Spin density and magnetic behavior (MB) corresponding to Mg concentrations (1–5%) and distance of oxygen vacancies. DV/NV abbreviates distant vacancy/near vacancy.

Mg (%)		1	2	3	4	5
MB (DV/NV)		FM/FiM	FM/FiM	FM/FiM	FM/FiM	FM/FiM
DV	Integrated Spin Density ($\hbar/2$)	9.651	9.652	9.607	9.641	9.643
	Integrated |Spin Density| ($\hbar/2$)	9.689	9.674	9.614	9.648	9.655
NV	Integrated Spin Density ($\hbar/2$)	5.696	5.664	3.058	5.837	5.712
	Integrated |Spin Density| ($\hbar/2$)	9.244	9.079	6.977	6.978	9.383

4. Conclusions

Magnetic nature of $Zn_{0.95-x}Mg_xNi_{0.05}O$ (x = 0, 0.01, 0.02, 0.03, 0.04, and 0.05) originated from Ni/Mg impurities and intrinsic oxygen vacancies were investigated through DFT calculations based on generalized gradient approximation with the PBE scheme. Oxygen vacancies as defects were taken into consideration by dislocating an oxygen atom that is near or distant from Ni atoms. The total energies increased (decreased) as Mg concentration increased for a non-defected (distant/near oxygen vacancy) system. Fermi energy appeared only at 1% Mg concentration which had the lowest total energy and a half-metallic behavior while the others showed metallic behavior in the absence of defects. Oxygen vacancies lead the system to gain FiM and FM behaviors near and distant vacancy cases, respectively which is independent of Mg concentration. The most number of states at the Fermi level was observed for 1% Mg-doped ZnNiO; this was a strong indication of the ferromagnetic behavior that was originated from the unpaired electrons around the Fermi level. However, Mg-doped ZnNiO showed a weak ferrimagnetic behavior for 2, 4, 5%, and antiferromagnetic for a 3% Mg doping ratio. FM was substantially originated from Ni(3d)-O(2p) for both defected and non-defected cases and Zn(3d) contributed to the magnetic state in the presence of oxygen vacancies. Distant vacancies enhanced the FM while near defected system showed FiM for all concentrations of Mg-doped to ZnNiO.

CRediT authorship contribution statement

I.P. Duru: Methodology, Software, Validation. **E. Ozugurlu:** Software, Writing - review & editing. **L. Arda:** Conceptualization, Methodology, Writing - original draft, Validation, Writing - review & editing, Supervision, Funding acquisition.

Declaration of Competing Interest

The authors declare that they have no known competing financial interests or personal relationships that could have appeared to influence the work reported in this paper.

Acknowledgment

This work was supported by the Scientific and Technical Research Council of Turkey (TUBITAK) through Project No: 115F472 and the Research Fund of Bahcesehir University (BAU-BAP.2018.02.16).

The authors would like to thank Dr. Muhammet Arucu and SİMULAB due to their valuable contribution during atomic calculations.

Appendix A. Supplementary data

Supplementary data to this article can be found online at https://doi.org/10.1016/j.jmmm.2020.166653.

References

[1] L. Arda, The effects of Tb doped ZnO nanorod: an EPR study, J. Magn. Magn. Mater. 475 (2019) 493–501.
[2] S.D. Senol, C. Boyraz, E. Ozugurlu, A. Gungor, L. Arda, Band gap engineering of Mg doped ZnO nanorods prepared by a hydrothermal method, Cryst. Res. Technol. 54 (3) (2019) 1800234.
[3] A. Nuruddin, J.R. Abelson, Improved transparent conductive oxide/p + /i junction in amorphous silicon solar cells by tailored hydrogen flux during growth, Thin Solid Films 394 (2001) 48.
[4] T. Minami, New n-type transparent conducting oxides, MRS Bull. 25 (2000) 38.
[5] G.P. Dransfield, Inorganic sunscreens, Radiat. Prot. Dosim. 91 (2000) 271.
[6] D.R. Clarke, Varistor ceramics, J. Am. Ceram. Soc. 82 (1999) 485.
[7] C. Boyraz, N. Dogan, L. Arda, Microstructure and magnetic behavior of (Mg/Ni) co-doped ZnO nanoparticles, Ceram. Int. 43 (17) (2017) 15986–15991.
[8] I.P. Duru, E. Ozugurlu, L. Arda, A first-principles study of magnetic properties of $Zn_{0.94}Mg_{0.01}Mn_{0.05}0$, Mater. Res. Express 6 (12) (2019) ab63f6.
[9] P.V. Dorpe, V.F. Motsnyi1, M. Nijboer, E. Goovaerts, V.I. Safarov, J. Das, W. Van Roy, G. Borghs, Jo De Boeck, Highly efficient room-temperature spin injection in a metal-insulator-semiconductor light-emitting diode, Jpn. J. Appl. Phys. 42 (2003) L502–L504.
[10] K. Sato, H. Katayamayoshida, Material designs for transparent ferromagnetic with ZnO based magnetic semiconductors, Jpn. J. Appl. Phys. 39 (2014) L555–L558.
[11] K. Ueda, H. Tabata, T. Kawai, Magnetic and electric properties of transition-metal-doped ZnO films, Appl. Phys. Lett. 79 (2001) 988–990.
[12] M. Bibes, A. Barthélémy, Oxide spintronics, IEEE Trans. Electron Devices 54 (2007) 1003–1023.
[13] J. Tang, C.-Y. Wang, L.-T. Chang, Y. Fan, T. Nie, M. Chang, W. Jiang, Y.-T. Chen, H.-J. Yang, H.-Y. Tuan, L.-J. Chen, K.L. Wang, Electrical spin injection and detection in Mn5Ge3/Ge/Mn5Ge3 nanowire transistors, Nano Lett. 13 (2013) 4036–4043.
[14] L.-T. Chang, C.-Y. Wang, J. Tang, T. Nie, W. Jiang, C.-P. Chu, S. Arafin, L. He, M. Afsal, L.-J. Chen, K.L. Wang, Electric-field control of ferromagnetism in Mn-doped ZnO nanowires, Nano Lett. 14 (2014) 1823–1829.
[15] R.B. Zhao, D.L. Hou, J.M. Guo, C.M. Zhen, G.D. Tang, Room-temperature ferromagnetism in Ni-doped ZnO powders, J. Supercond. Nov. Magn. 23 (2010) 1261–1265.
[16] X. Liu, F. Lin, L. Sun, W. Cheng, Doping concentration dependence of room-temperature ferromagnetism for Ni-doped ZnO thin films prepared by pulsed-laser deposition, Appl. Phys. Lett. 88 (2006) 062508.
[17] J.B. Cui, U.J. Gibson, Electrodeposition and room temperature ferromagnetic anisotropy of Co and Ni-doped ZnO nanowire arrays, Appl. Phys. Lett. 87 (2005) 1341a08.
[18] H. Jr, C.S. He, L.J. Lao, D. Chen, Z.L. Wang Davidovic, Large-scale Ni-doped ZnO nanowire arrays and electrical and optical properties, J. Am. Chem. Soc. 127 (2005) 16376–16377.
[19] T. Wakano, N. Fujimura, Y. Morinaga, N. Abe, A. Ahida, T. Ito, Magnetic and magneto-transport properties of ZnO: Ni films, Phys. E 10 (2001) 260–264.
[20] T. Al-Harbi, Hydrothermal synthesis and optical properties of Ni-doped ZnO hexagonal nanodiscs, J. Alloys Compd. 509 (2011) 387–390.
[21] C. Cheng, G. Xu, H. Zhang, Y. Luo, Hydrothermal synthesis Ni-doped ZnO nanorods with room-temperature ferromagnetism, Mater. Lett. 62 (2008) 1617–1620.
[22] Z. Yin, N. Chen, F. Yang, S. Song, C. Chai, J. Zhong, H. Qian, K. Ibrahim, Structural, magnetic properties and photoemission study of Ni-doped ZnO, Solid State Commun. 135 (2005) 430–434.
[23] L. Arda, M. Açıkgöz, A. Güngör, Magnetic and microstructure properties of Ni-doped ZnO films and powder by sol-gel process, J. Supercond. Nov. Magn. 25 (2012) 2701–2705.
[24] N. Dogan, A. Bingolbali, L. Arda, Preparation, structure and magnetic characterization of Ni-doped ZnOnano-particles, J. Magnet. Magnet. Mat. 373 (2015) 226–230.
[25] Z.K. Heiba, M.B. Mohamed, L. Arda, N. Dogan, Cation distribution correlated with magnetic properties of nanocrystalline gadolinium substituted nickel ferrite, J. Magn. Magn. Mater. 391 (2015) 195–202.
[26] R. Viswanatha, Y. Arthoba Nayaka, C.C. Vidyasagar, T.G. Venkatesh, Structural and optical properties of Mg-doped ZnO nanoparticles, J. Chem. Pharm. Res. 4 (4) (2012) 1983–1989.
[27] A. Kołodziejczak-Radzimska, T. Jesionowski, Zinc oxide from synthesis to application: a review, Mater. MDPI 7 (4) (2014) 2834–2881.
[28] A.-H. El Foulani, A. Aamouche, F. Mohseni, J.S. Amaral, D.M. Tobaldi, R.C. Pullar, Effect of surfactants on the optical and magnetic properties of cobalt-zinc ferrite $Co_{0.5}Zn_{0.5}Fe_2O_4$, J. Alloys Compd. 774 (2019) 1250–1259.
[29] M. Rajendran, R.C. Pullar, A.K. Bhattacharya, D. Das, S.N. Chintalapudi, C.K. Majumdar, Magnetic properties of nanocrystalline CoFe2O4 powders prepared at room temperature: variation with crystallite size, J. Magn. Magn. Mater. 233 (2001) 71–83.
[30] P.S. Vachhani, A.H. Rawal, A.K. Bhatnagar, R.J. Choudhary, D.M. Phase, P. Rajput, S.N. Jha, D. Bhattacharyya, Studies on structural, optical and magnetic properties of Mg- and Li-doped Cu:ZnO films, Mater. Res. Express 4 (2017) 076109.
[31] Javed Iqbal, Baiqi Wang, Xiaofang Liu, Yu Dapeng, B. He, Ronghai Yu, Oxygen-vacancy-induced green emission and room-temperature ferromagnetism in Ni-doped ZnO nanorods, New J. Phys. 11 (2009) 063009.
[32] S.J. Clark, M.D. Segall, C.J. Pickard, P.J. Hasnip, M.J. Probert, K. Refson, M.C. Payne, First-principles methods using CASTEP, Z. Kristallogr. 220 (5–6) (2005) 567–570.
[33] Y. Wang, T. Hou, S. Tian, S.-T. Lee, Y. Li, Influence of doping effect on zinc oxide by first-principles studies, J. Phys. Chem. C 115 (15) (2011) 7706–7716.
[34] I.P. Duru, E. Ozugurlu, L. Arda, Size effect on magnetic properties of $Zn_{0.95-x}Mg_x Ni_{0.05}$ O nanoparticles by Monte Carlo simulation, Ceramics Int. 45 (5) (2019) 5259–5265.
[35] B. Haq, R. Ahmed, Structural and electronic properties of Ni-doped ZnO in zinc-blende phase: a DFT investigations, AIP Conf. Proc. 54 (2012) 1482.
[36] B. Haq, R. Ahmed, G. Abdelatif, A. Shaari, F. Butt, M. Kanoun, S. Goumri-Said, Dominant ferromagnetic coupling over antiferromagnetic in Ni-doped ZnO: first-principles calculations, Front. Phys. 11 (1) (2016) 117101.
[37] Weng Zhen-Zhen, et al., Effect of oxygen vacancy defect on the magnetic properties of Co-doped ZnO, Chin. Phys. B 20 (2011) 2.
[38] Qingyu Hou, Liu Yajing, Wenling Li, Effects of Co doping and O vacancy on the magnetism of ZnO, Solid State Commun. 306 (2020) 113775.
[39] Qian Wang, et al., Vacancy-Induced Magnetism in ZnO Thin Films and Nanowires, Physical review, B, Condensed matter 77 (2008) 20.
[40] J.M.D. Coey, M. Venkatesan, C.B. Fitzgerald, Donor impurity band exchange in dilute ferromagnetic oxides, Nat. Mater. 4 (2005) 173.
[41] J.E. Jaffe, T.C. Droubay, S.A. Chambers, Oxygen vacancies and ferromagnetism in $Co_xTi_{1-x}O_{2-x-y}$, J. Appl. Phys. 97 (2005) 73908.
[42] H. Weng, X. Yang, J. Dong, H. Mizuseki, M. Kawasaki, Y. Kawazoe, Electronic structure and optical properties of the Co-doped anatase studied from first principles, Phys. Rev. B 69 (2004) 125219.